CHAPTER

12 Short Waves*

12.1 Introduction

As was seen in the previous chapter, classical finite element methods can deal relatively easily with linear waves in two and three dimensions, when there are few wavelengths in the problem domain. But many problems of practical importance contain many wavelengths. The computational demands of conventional numerical methods for an accurate solution cannot be met. So in recent years, attention has turned to new types of finite elements for such problems. Similar special variations have also been developed for other numerical methods, such as boundary elements. Surveys of these methods are available [1,2]. A variety of new finite elements have been developed, and they will be surveyed briefly in this chapter. A common feature is that most incorporate more of our knowledge of waves and wave behavior into the algorithm. The problem of short waves in a large domain is part of the general class of multiscale problems [3,4]. That is, the problem is of large scale, but the overall behavior is significantly influenced by small-scale behavior. Other important examples are the behavior of structures composed of materials with microstructure, for example composites or concrete, and turbulent flows. In the latter the details of the flow, with very small length scales, strongly influence the behavior of the entire system.

12.2 Background

A prime example of a short-wave problem is that of radar waves incident upon an aircraft. The wavelength of the radio wave may be of the order of several mm, whereas the size of the aircraft is of the order of tens of meters. Since about 10 degrees of freedom are needed per wavelength in conventional numerical models this gives a scale factor of over 1000. Classical finite element methods generate large systems of equations with literally astronomical numbers of unknowns for the solution of such problems. This makes them virtually intractable. If we imagine a computational domain around

*Contributed by Peter Bettess, Formerly Professor School of Engineering, University of Durham, UK.

Finite Element Meth Fluid Dynam 7E, Volume 3. http://dx.doi.org/10.1016/B978-1-85617-635-4.00012-1

an aircraft of a cube of 20 m per side and a wavelength of the incident wave of 2 cm, it is possible to compute the size of the computational problem. The above model requires $n = 10^{12}$ nodal variables, all complex. The semi-bandwidth of a finite element model would be $b = 10^8$ degrees of freedom, leading to a storage requirement for a classical direct solver of $nb = 10^{20}$ complex words, or 1.6×10^{21} bytes. The number of complex arithmetic operations would be $nb^2/2 = 0.5 \times 10^{27}$. Twenty meters is not large for a model size and 2 cm is not small for a radar wavelength. It corresponds to a frequency of about 15 GHz, and radar can operate at higher frequencies. So it can be seen that conventional methods, even on supercomputers, struggle to make an impact on such problems. But the solutions are of great practical interest.

For most short-wave problems the frequency domain solutions are of the most interest. Even in radar applications, where the radar beam is transient, it still endures for many wave cycles so the problem is really in the frequency domain. There are important short-wave transient problems, but these are in the minority. There are essentially two approaches to frequency domain problems. The first is to iterate a general transient solution to a steady state. The second is to factor the frequency out of the problem and to operate on the resulting complex equations.

1. **Time domain solutions.** These methods imply some kind of stepping forward in time, usually based on a finite difference in time scheme. Many different schemes have been proposed. The advantage of this approach is that any transient problem can be solved. If an explicit scheme is used, together with a diagonal mass matrix, then the computation involved in a time step is very small, and the storage requirements are very small. Such methods are explained in detail in Ref. [5] and in Chapter 3 of the present book.
2. **Frequency domain solutions.** These methods solve the response for a given frequency. All terms in the problem are factored by $\exp(i\omega t)$, as explained in the previous chapter. The advantage is that a single solution of a complex system matrix gives a complete solution at all times. The disadvantage is that they cannot directly solve transient problems, although Fourier transforms can be used to move from a set of frequency domain solutions to a transient solution, for linear problems. The complex system matrix to be solved, though sparse for finite elements, is very large and direct solutions are very computationally expensive. Such problems have been described in Ref. [5].

In recent years the problem described above, that of the limitation in the short waves, has been subjected to attack from a number of different directions, which have shown considerable promise. It is fair to say that in the last 10 years, the wavelengths in the scattering problems which can be solved have decreased dramatically. As a consequence the frequencies have increased.

The historical trend is toward tailoring the numerical algorithms to the known nature of the wave problem, and to use the best possible algorithms, for example in integrating the various matrices which arise.

12.3 Errors in wave modeling

It was earlier stated that about 10 degrees of freedom are needed to model each wavelength. However that is an oversimplification. There are two sorts of errors which arise from wave modeling using polynomials. These are *local* errors and *pollution* errors. Error estimates for these errors have been given by several authors [6–9]. Ihlenburg and Babuška [6] give expressions for the error, e, in the H^1-seminorm, in a domain of *unit length*, as

$$e <= C_1(p)\left(\frac{hk}{2p}\right)^m + C_2(p)k\left(\frac{hk}{2p}\right)^{m+1} \tag{12.1}$$

where p is the order of the finite element polynomial, h is the element size, and m is the minimum of l and p, where $l + 1$ is the regularity of the exact solution. C_1 and C_2 are constants depending only upon p. The first term in Eq. (12.1) is the *local* error and the second term is the *pollution* error, which increases with k, even for (hk) fixed. If the domain is large the second term will come to dominate. It is evident from Eq. (12.1) that, other things being equal, it is desirable to have the highest possible order of polynomial in the finite element, if we seek to minimize the error for a given discretization. The pollution error can be thought of as an error in the numerical value for the wavelength. Obviously, the larger the number of wavelengths in a problem then the more the errors from this source will accumulate.

12.4 Recent developments in short-wave modeling

There have been several important developments in recent years, which have enabled the finite element method to be applied to wave scattering problems with much smaller wavelengths, or at much higher frequencies. The approaches can be outlined as follows:

1. Conventional finite element polynomials, with a transient solution scheme, possibly with characteristic-based algorithms
2. Finite elements which incorporate the wave shape
   - **(a)** Shape functions using *products* of waves and polynomials
   - **(b)** Shape functions using *sums* of waves and polynomials
   - **(c)** Ultra weak formulations
   - **(d)** Trefftz-type finite elements which incorporate wave shapes
3. Spectral schemes
4. Discontinuous Galerkin methods in transient schemes

There have been similar developments within the boundary element field, which are too extensive to discuss here. Other surveys are available [1,2].

12.5 Transient solution of electromagnetic scattering problems

The penalty in using a fine mesh of conventional finite elements in solving wave problems, referred to above, is the storage and solution of the system matrix. The approach of Morgan et al. [10,11] is to not assemble and solve the system matrix, and to treat the problem as transient. The Maxwell equations are

$$\varepsilon_0 \frac{\partial \mathbf{E}}{\partial t} = \text{curl}\mathbf{H} \quad \text{and} \quad \mu_0 \frac{\partial \mathbf{H}}{\partial t} = -\text{curl}\mathbf{E} \tag{12.2}$$

where **E** and **H** are the electric and magnetic field intensity vectors respectively. The equations are combined and expressed in the conservation form

$$\frac{\partial \mathbf{U}}{\partial t} = \sum_{j=1}^{3} \frac{\partial \mathbf{F}^j}{\partial x_j} = \mathbf{0} \quad \text{where} \quad \mathbf{U} = \begin{bmatrix} \mathbf{E} \\ \mathbf{H} \end{bmatrix} \tag{12.3}$$

and the flux vectors, **F**, are derived from the curl operators. That is

$$\begin{aligned} \mathbf{F}^1 &= \left[0, H_3, -H_2, 0, -E_3, E_2\right]^T \\ \mathbf{F}^2 &= \left[-H_3, 0, H_1, E_3, 0, -E_1\right]^T \\ \mathbf{F}^3 &= \left[H_2, -H_1, 0, -E_2, E_1, 0\right]^T \end{aligned} \tag{12.4}$$

The algorithm used is the characteristic-Galerkin (or Lax-Wendroff) method as described in Chapter 2. Details of the algorithm as applied to the electromagnetic problem are given by Morgan et al. Improved CPU efficiency and reduced storage requirements are obtained by the use of a representation in which each edge of the tetrahedral mesh is numbered and the data structure employed provides the numbers of the two nodes which are associated with each edge. Because of the massive computations needed for problems of scattering by short waves, parallel processing has also been used. The problem of radar scattering by an aircraft is shown in Fig. 12.1a and 12.1b shows the radar cross-section obtained for the aircraft.

Morgan et al. present results for electromagnetic waves scattered by an aircraft of length 18 m, for a wavelength of 1 m. The model was run on a CRAY parallel computer and had about 1,500,000 elements.

12.6 Finite elements incorporating wave shapes

In these elements the usual polynomial shape functions are extended with functions which enhance the solution space used in the element. The first attempt to do this was the infinite elements of Bettess and Zienkiewicz [12,13]. The first attempt on *finite* elements was that of Astley [14,15], using his wave envelope, or complex conjugate weighting method. For more details, see Chapter 11, Section 11.12. Following

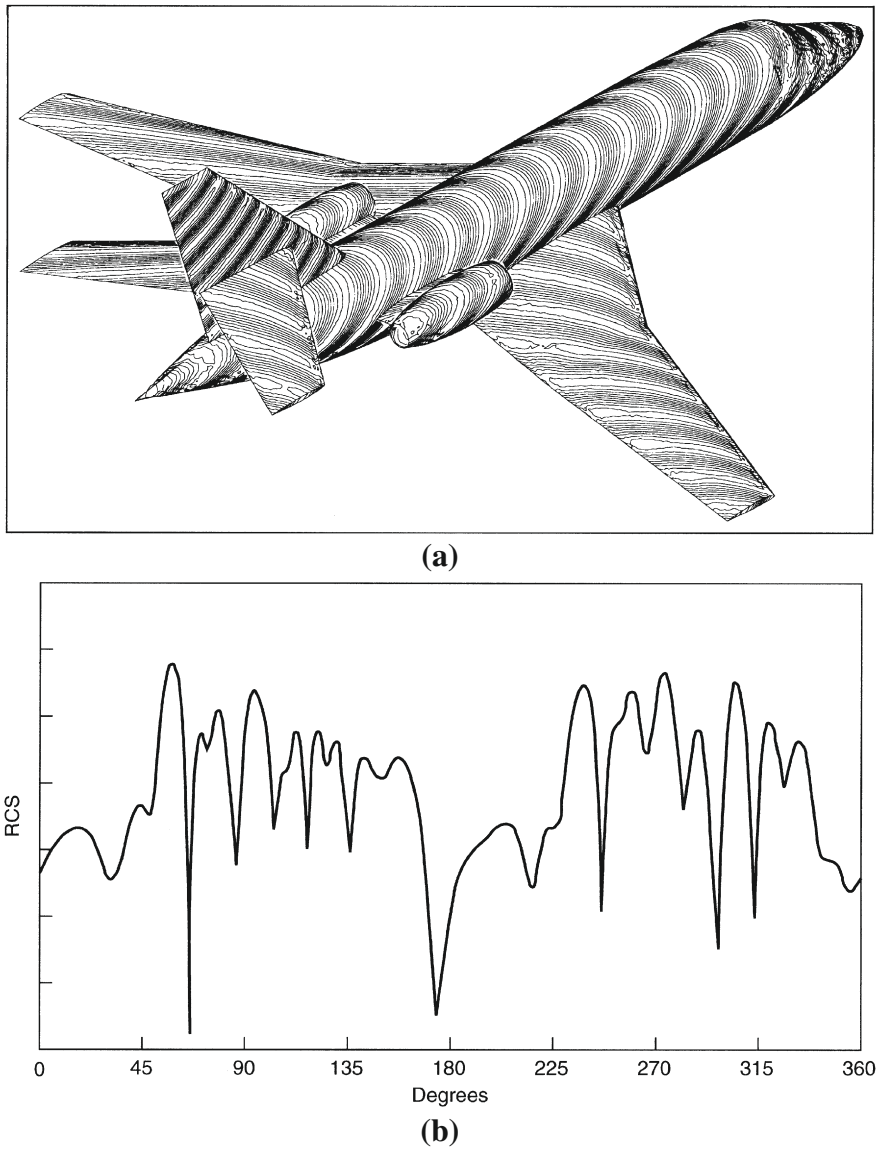

FIGURE 12.1
Scattering of a plane wavelength 2 m by a perfectly conducting aircraft of length 18 m: (a) waves impacting aircraft, (b) computed distribution of radar cross-section (RCS), Morgan [10].

Astley's wave envelope technique, Chadwick et al. [16] attempted to develop wave envelope finite elements in which the wave direction was unknown, *a priori*, and to iterate for the correct wave direction, using some type of residual. In the above

methods single waves were included in the elements either in a radial or some predefined direction.

Chadwick's approach had some success but has difficulties. The next step was the method proposed by Melenk and Babuška [17,18] in which *multiple* plane waves are used. This is categorized as a form of the partition of unity finite element method (see Chapter 3 of Ref. [5]). Melenk and Babuška demonstrated that if such shape functions are used the method works for a plane wave propagated through a square mesh of square finite elements, even when the direction of the wave was not included in the nodal directions. The set of plane waves is complete [19], so the choice is rational. Other wave functions have been suggested such as cylindrical waves, or a series of Hankel functions. Melenk and Babuška [17,18] and Huttunen et al. [20,21] consider various choices for the wave functions. Mayer and Mandel [22] have also used shape functions which incorporate the wave shape.

Similar ideas were also developed in the boundary integral method by de La Bourdonnaye, under the title of *microlocal discretization* [23,24]. All the methods mentioned above use trial functions, or shape functions, formed from the product of the usual polynomial shape functions and plane (or almost plane) waves. One of the problems with this approach is that the integrations over the element domain may become computationally intensive. It is also possible to *add* the wave solutions to the polynomial element shape functions or to use different methods which sidestep the integration difficulties (see Section 12.6.3.).

12.6.1 Shape functions using products of polynomials and waves

Laghrouche and Bettess applied the method originated by Melenk and Babuška [17,18] to a range of wave problems, and enjoyed some success [25,26]. The starting point is the standard Galerkin weighted residual form of the Helmholtz equation, which leads to

$$\int_{\Omega} \left(-\nabla^{\mathrm{T}} W(\nabla\phi + k^2 W\phi\right) \mathrm{d}\Omega + \int_{\Gamma} W(\nabla\phi)^{\mathrm{T}} \mathbf{n} \mathrm{d}\Gamma = 0 \tag{12.5}$$

The element approximation is now taken as

$$\phi = \sum_{a=1}^{n} \sum_{l=1}^{m} N_a \psi_l A_a^l \tag{12.6}$$

where N_j are the normal polynomial element shape functions,

$$\psi_l = \mathrm{e}^{\mathrm{i}k(x\cos\theta_l + y\sin\theta_l)} \tag{12.7}$$

n is the number of nodes in the element, and m is the number of directions considered at each node. The shape function consists of a set of plane waves traveling in different directions, the nodal degrees of freedom corresponding to the amplitudes of the different waves, and the normal polynomial element shape functions allowing a variation in the amplitude of each wave component within the finite element. The derivatives of the shape and weighting functions can be obtained in the normal way,

but these now also include derivatives of the wave shapes. The new shape function, P_i, gives

$$\begin{Bmatrix} \dfrac{\partial P_{(a-1)m+l}}{\partial x} \\ \dfrac{\partial P_{(a-1)m+l}}{\partial y} \end{Bmatrix} = \left[\begin{Bmatrix} \dfrac{\partial N_a}{\partial x} \\ \dfrac{\partial N_a}{\partial y} \end{Bmatrix} + \mathrm{i}kN_a \begin{Bmatrix} \cos\theta_l \\ \sin\theta_l \end{Bmatrix} \right] \psi_l \tag{12.8}$$

The global derivatives are obtained in the usual way from the local derivatives, using the inverse of the Jacobian matrix. The element stiffness and mass matrices are

$$K_{rs} = \int_\Omega (\nabla W_r)^{\mathrm{T}} \nabla P_s \, \mathrm{d}\Omega \quad M_{rs} = \int_\Omega W_r P_s \, \mathrm{d}\Omega \tag{12.9}$$

where r and s are integers which vary over the range of $1, 2, \ldots, (n \times m)$. When calculating the element matrices, the integrals encountered are of the form (for a quadrilateral element)

$$I_{al} = \int_{-1}^{1} \int_{-1}^{1} f(\xi, \eta) \, \mathrm{e}^{\mathrm{i}k(x\cos\theta_a + y\sin\theta_a)} \, \mathrm{e}^{\mathrm{i}k(x\cos\theta_l + y\sin\theta_l)} \, \mathrm{d}\xi \, \mathrm{d}\eta \tag{12.10}$$

This integral has often been performed numerically. But when the waves are short, many Gauss-Legendre integration points are needed. Typically about 10 integration points per wavelength are needed. Laghrouche and Bettess solve a range of wave diffraction problems, including that of plane waves diffracted by a cylinder. The mesh and the results are shown in Fig. 12.2. As can be seen the results are in good agreement with the analytical series solution. In this problem $ka = 8\pi$, $\lambda = 0.25a$, radius of cylinder, $a = 1$, and the mesh extends to $r = 7a$. For a conventional radial finite element mesh, the requirement of 10 nodes per wavelength would lead to a mesh with 424,160 degrees of freedom. But in the results shown, with 36 directions per node and 252 nodes there are only 9072 degrees of freedom. The dramatic reduction in the number of variables has prompted investigation and development of the method. The method still has a number of uncertainties regarding the conditioning of the system matrix and the stability of the technique. Various approaches have been suggested to reduce the cost of integrating the element matrix.

For the choice of a plane wave basis, any term in the element matrix can be written as the product of two plane waves, and a polynomial term. The general integral which arises, in two dimensions, is of the form

$$\int_\Omega f(\xi, \eta) e^{ig(\xi,\eta)} \mathrm{d}\Omega \tag{12.11}$$

where ξ and η are the local coordinates, $f(\xi, \eta)$ is a rational function which reduces to a polynomial if the Jacobian is constant, $g(\xi, \eta)$ is some function related to the element mapping, and Ω is the element domain. If the Jacobian is constant, then $g(\xi, \eta) = \alpha\xi + \beta\eta$ (α and β being constants), which greatly simplifies the integrations. Such integrals are highly oscillatory and difficult to evaluate. The first analyses using such elements used large numbers of Gauss-Legendre integration points [17,18,25,26]. The approach of Ortiz and Sanchez [27] is to combine the two plane waves traveling in

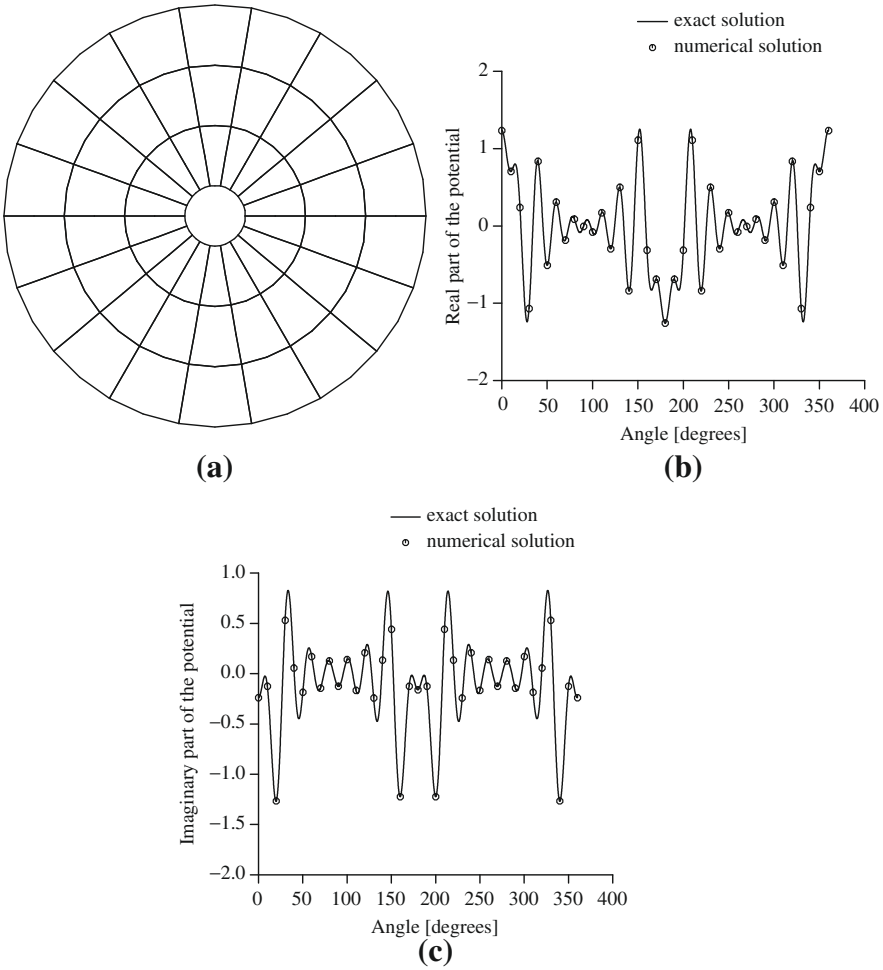

FIGURE 12.2

Short waves diffracted by a cylinder, modeled using special finite elements [26]; (a) cylinder mesh; (b) real potential; (c) imaginary potential. *Reprinted from Ref. [26], with permission from Journal of Computational Acoustics.*

directions θ_1 and θ_2 to the x-axis, to give a single wave traveling in the mean direction, $\theta = (\theta_1 + \theta_2)/2$ with a local wavenumber, k' given by $k' = 2k \cos(\theta_1 - \theta_2)/2$. The integral then takes the simpler form

$$\int_{\Omega} f(\xi, \eta) e^{i\gamma\xi} \, d\Omega \tag{12.12}$$

where in Eq. (12.12), ξ is oriented in the mean wave direction, η is perpendicular, and γ depends on the local wavenumber and element geometry. Ortiz and Sanchez used this result to develop a special integration scheme in the direction of the wave

resultant, ξ, which contains all the oscillatory effects, in combination with classical integration in the orthogonal η direction, where the variation is of a polynomial form. This has the advantage that the integration of the oscillatory function has been reduced by one dimension. The price that has to be paid is that a new local coordinate system must be set up for each pair of wave directions, and the limits of integration are no longer simple. To date their approach has only been applied to linear triangular elements. Whether the limits of integration will be easy to manipulate with higher-order elements, and in three dimensions, has not yet been investigated. Ortiz has extended his approach to refraction problems and this is described below in Section 12.7.

Another approach to the integral of Eq. (12.10) was suggested by Bettess et al. [28]. In Bettess et al.'s method the constant Jacobian for simpler finite elements is exploited to transform the integrations into the local coordinates. This integral takes the following specific form for the linear triangular finite element:

$$\int_0^1 \int_0^{1-\xi} f(\xi, \eta) e^{i\alpha\xi} e^{i\beta\eta} \, \mathrm{d}\eta \, \mathrm{d}\xi \tag{12.13}$$

In the above ξ and η are the local coordinates, and $f(\xi, \eta)$ is a polynomial. Unfortunately the resulting expressions, though straightforward, become complicated and it is almost essential to use computer algebra [28]. Nevertheless an integration scheme can be developed. Both the Ortiz and Bettess et al. approaches have been demonstrated to give large reductions in computer time, when the waves become short. Bettess et al. have also demonstrated that the integrations over rectangular and cuboid finite elements can be greatly simplified. Their method has also been applied to tetrahedral element integrations (unpublished work). The other feature of these approaches is that although the integration of each finite element matrix is computationally intensive, the calculations are highly parallelizable. There is no difficulty in obtaining an n times speed-up on a computer with n processors. Any repetition in the element geometries can also be exploited.

A feature of these partition of unity finite elements (PUFE) is that the system matrix is often ill-conditioned. This has concerned some authors [18,22]. Strouboulis et al. [4] suggest that in this general class of methods the equations may be ill-conditioned, but that this is not necessarily a bad thing. The final results may be acceptable, even if the coefficients of the wave components are not unique. Astley [29] has analyzed the conditioning of the element matrices, for some simple cases, and has evolved a semi-empirical rule relating condition number, number of wave directions, and wavenumber. Babuška et al. [17,18] also consider *a posteriori* error estimation for such elements. Mayer and Mandel [22] also discuss strategies for selecting wave directions. The method can be extended to three dimensions [29,30] and can be linked to conventional infinite elements [31].

12.6.2 Shape functions using sums of polynomials and waves

The complications arising from the integration of products of shape functions and wave functions can be eliminated by introducing the waves in a different form, for

example by adding the set of waves to the conventional shape function polynomials. Two of these approaches will now be considered. These are

1. The discontinuous enrichment method of Farhat [32–34]
2. The ultra weak variational formulation of Després and Cessenat [35,36], and Huttunen and Monk [20,21]

12.6.3 The discontinuous enrichment method

The Farhat et al. [32–34] approach uses the original polynomial shape function and *adds* to it the set of plane waves. (This is in contrast to the Babuška and Melenk approach, described above in Section 12.3, in which the plane waves are *multiplied* by the polynomials.) Continuity with adjacent elements is enforced weakly by using Lagrange multipliers. The integrations relating to the plane waves, which Farhat terms *enrichment functions*, can be reduced to integrations along element boundaries. Moreover, these terms can be eliminated from the element matrix, by the use of static condensation. There are three sets of variables in the finite elements:

1. $\boldsymbol{\phi}^P$, the usual nodal variables for the finite element polynomial which is used.
2. $\boldsymbol{\phi}^E$, the variables relating to the solutions of the Helmholtz equation used for "enrichment." These may be coefficients of plane waves, Hankel sources, or other wave solutions.
3. $\mathbf{p}$, the Lagrange variables which are defined along the edges of the element.

The boundary value problem is put in variational form. The Lagrange multipliers which enforce compatibility are defined as the trace, or outward normal, of vectors $\mathbf{p}$. The contribution to the functional for an element is then

$$\Pi(u, \mathbf{p}) = \frac{1}{2}\int_{\Omega^e} \left(\nabla^T\phi \cdot \nabla\phi - k^2\phi^T\phi\right) \mathrm{d}\Omega - \int_{\Gamma^e} \mathbf{p}\cdot\mathbf{n}\phi \,\mathrm{d}\Gamma \tag{12.14}$$

The potential ϕ is split into the polynomial and enrichment functions as described above. That is, $\phi = \phi^P + \phi^E$. The resulting element matrix is similar, but not identical to those shown in Chapter 11 of Ref. [5]. It takes the form

$$\begin{bmatrix} \mathbf{K}^{PP} & \mathbf{K}^{PE} & \mathbf{K}^{PC} \\ \mathbf{K}^{EP} & \mathbf{K}^{EE} & \mathbf{K}^{EC} \\ \mathbf{K}^{CP} & \mathbf{K}^{CE} & \mathbf{0} \end{bmatrix} \begin{Bmatrix} \boldsymbol{\phi}^P \\ \boldsymbol{\phi}^E \\ \mathbf{p}^C \end{Bmatrix} \tag{12.15}$$

where the various matrices $\mathbf{K}^{ij}$ arise from the variational statement of the Helmholtz equation. Because the "enrichment" variables $\boldsymbol{\phi}^E$ are only defined internally to each element, they can be eliminated at the element level using static condensation. This leads to a final element matrix with only polynomial $\boldsymbol{\phi}^P$ and Lagrange multipliers $\mathbf{p}$ as variables. The element matrix then takes the form

$$\tilde{\mathbf{k}}^e = \begin{bmatrix} \tilde{\mathbf{k}}^{PP} & \tilde{\mathbf{k}}^{PC} \\ \tilde{\mathbf{k}}^{CP} & \tilde{\mathbf{k}}^{CC} \end{bmatrix} \tag{12.16}$$

where

$$\tilde{\mathbf{k}}^{PP} = \tilde{\mathbf{k}}^{PP} - \tilde{\mathbf{k}}^{PE}\left(\tilde{\mathbf{k}}^{EE}\right)^{-1}\tilde{\mathbf{k}}^{EP}, \quad \tilde{\mathbf{k}}^{PC} = \tilde{\mathbf{k}}^{PC} - \tilde{\mathbf{k}}^{PE}\left(\tilde{\mathbf{k}}^{EE}\right)^{-1}\tilde{\mathbf{k}}^{EC} \tag{12.17}$$

$$\tilde{\mathbf{k}}^{CP} = \tilde{\mathbf{k}}^{CP} - \tilde{\mathbf{k}}^{CE}\left(\tilde{\mathbf{k}}^{EE}\right)^{-1}\tilde{\mathbf{k}}^{EP}, \quad \tilde{\mathbf{k}}^{CC} = -\tilde{\mathbf{k}}^{CE}\left(\tilde{\mathbf{k}}^{PP}\right)^{-1}\tilde{\mathbf{k}}^{EC} \tag{12.18}$$

The vectors **p** used to generate the Lagrange multiplier must be chosen correctly. For a triangle element Farhat gives

$$\mathbf{p}(x, y) = s\begin{Bmatrix} c_1 + c_3 x \\ c_2 + c_3 y \end{Bmatrix} \tag{12.19}$$

where c_i are constants. This gives a constant Lagrange multiplier along the element edge. Farhat points out that because the enrichment functions satisfy the homogeneous Helmholtz equation, the integrals over the domain can be reduced to integrals over the boundaries of the elements. The Lagrange multiplier terms can also be scaled to improve matrix conditioning. These are all very attractive features of the method. Farhat also reports better conditioning of the system matrix with this approach. The results given in his report are all quite academic, being mostly concerned with the propagation of plane waves through square meshes of square elements. Some studies of errors are given. Errors are very low when the plane wave is traveling in one of the directions used for the plane wave basis, or a direction close to it. For other directions, although the errors are larger, they are much smaller than in conventional Galerkin finite elements.

12.6.4 Ultra weak formulation

Another promising approach is termed the ultra weak formulation. Among the leading innovators here have been Després [35], Cessenat and Després [36], and Huttunen et al. [20,21]. To quote Huttunen, "In this approach integration by parts is used to derive a variational formulation that weakly enforces appropriate continuity conditions between elements via impedance boundary conditions." The significant advantage of this approach is that the integrations over each element can be obtained in closed form. This is because the variational principle used relies on a test function which satisfies the Helmholtz equation. As a result all the integrals over the element domain vanish, leaving only integrals along element boundaries, which enforce compatibility between elements. This contrasts with the integration of classical plane wave basis (or other wave basis) element matrices which can be very computer intensive. As in the PUFE method described above, ill conditioning of the system matrix may be a problem. Cessenat and Després [36] developed the mathematics of the procedure and applied it to the scattering of electromagnetic waves by a NACA 0012 aerofoil, at 1500 MHz. Huttunen et al. [20] considered an inhomogeneous version of the Helmholtz equation, which looks similar to the shallow-water wave equation, Eq. (11.2):

$$\nabla \cdot \left(\frac{1}{\rho}\nabla u\right) + \frac{k^2}{\rho}u = 0 \quad \text{in} \quad \Omega \tag{12.20}$$

$$\left(\frac{1}{\rho}\frac{\partial u}{a\partial \nu} - i\sigma u\right) = Q\left(-\frac{1}{\rho}\frac{\partial u}{a\partial \nu} - i\sigma u\right) + g \quad \text{on} \quad \Gamma \tag{12.21}$$

where Ω is the domain and Γ is the smooth boundary. Both $\rho(x_1, x_2)$, and $k(x_1, x_2)$ are functions of position. Q is a parameter defined on the boundary, Γ, $Q \leq 1$. Although this formulation allows for spatial variation in ρ and k, in practice the treatment in the paper takes them to be piecewise constant in each element. The method is applied to problems in which different zones have different wave speeds. Richardson [27] and stabilized bi-conjugate gradient iterative methods were used for solving the system matrix. Huttunen et al. [21] have also applied the method to elastic wave problems.

Cessenat and Després [36] present results for the scattering of an electromagnetic wave of frequency 1500 MHz by a NACA 0012 aerofoil. The mesh was laid down in three layers around the aerofoil. A total of 2976 elements with 1615 nodes were used. Figure 12.3 shows the radar cross-section of the aerofoil.

Huttunen et al. solved a number of example problems [20], using the ultra weak variational method, including that shown in Figs. 12.4–12.6. This is an inner domain of radius 5 cm, with a wave speed of 3000 m s^{-1} and a computational domain of radius 10 cm, with a wave speed of 1500 m s^{-1}. A cylindrical wave source, of the

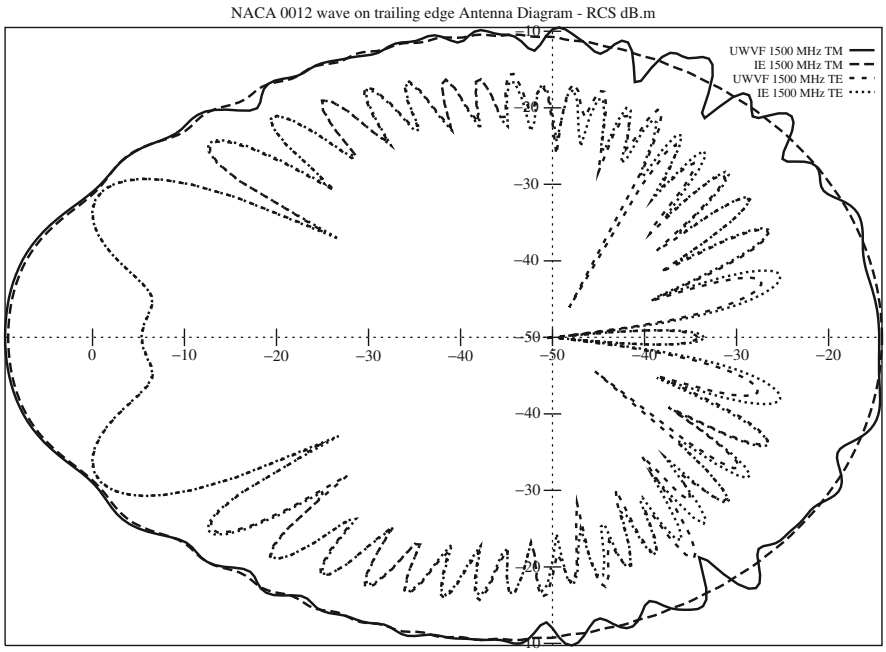

FIGURE 12.3

Radar cross-section for *NACA 0012* on trailing edge at 1500 MHz [36]. Comparisons of UWVF and boundary integral results for frequency 1500 MHz, and TM and TE polarizations. *Figure reprinted from Ref. [36], with permission from SIAM.*

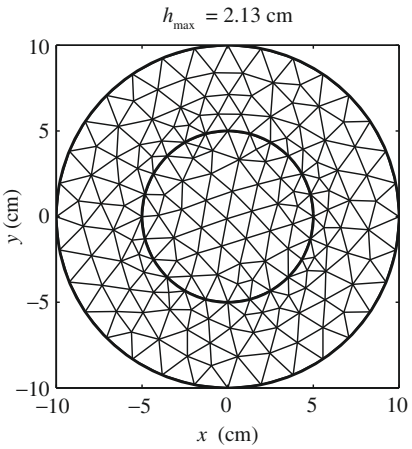

FIGURE 12.4

Ultra weak variational element mesh, Huttunen et al. [20]. *Reprinted from Ref. [20], with permission from Elsevier.*

form

$$u^{in} = \frac{i}{4} H_0^{(1)}\left(k_2 r\right) \tag{12.22}$$

has an origin, for the radius, r, located at $x = -11$ cm, $y = 0$ cm. The maximum element size is $h_{max} = 2.13$ cm. Figure 12.5 shows the analytical solution compared with the solution obtained using the ultra weak variational formulation (UWVF), for $f = 250$ kHz. Huttunen et al. report good results for frequencies up to 450 kHz, corresponding to about six wavelengths per element. Two strategies were used, one of uniform number of bases for each element and the other in which the number of bases was dictated by the condition number. The details of the strategy are too complicated to report here. However better results were obtained by using the varying number of basis functions. The relative errors at different frequencies and the condition number are shown in Fig. 12.6.

12.6.5 Trefftz-type finite elements for waves

There is now a considerable literature on the Trefftz-type finite (or T-element) methods. Two of the key workers in this field are Jirousek and Herrera. Survey papers are available [37,38]. It is assumed that the scattering form of the Helmholtz equation is to be solved. The theory has been developed by Jirousek and Stojek [39,40]. Background theory on suitable functions for the Trefftz method and T-completeness is given by Herrera [41]. The method has also been applied by Cheung et al. [42] to wave scattering and wave force problems. The theory here follows Stojek [40]. The problem domain Ω is divided into n computational subdomains, Ω_k, each with their own local coordinate system, (r_k, θ_k). In each subdomain, Ω_k, the total wave potential is written as ϕ_k. It is assumed to be an approximate solution which satisfies the

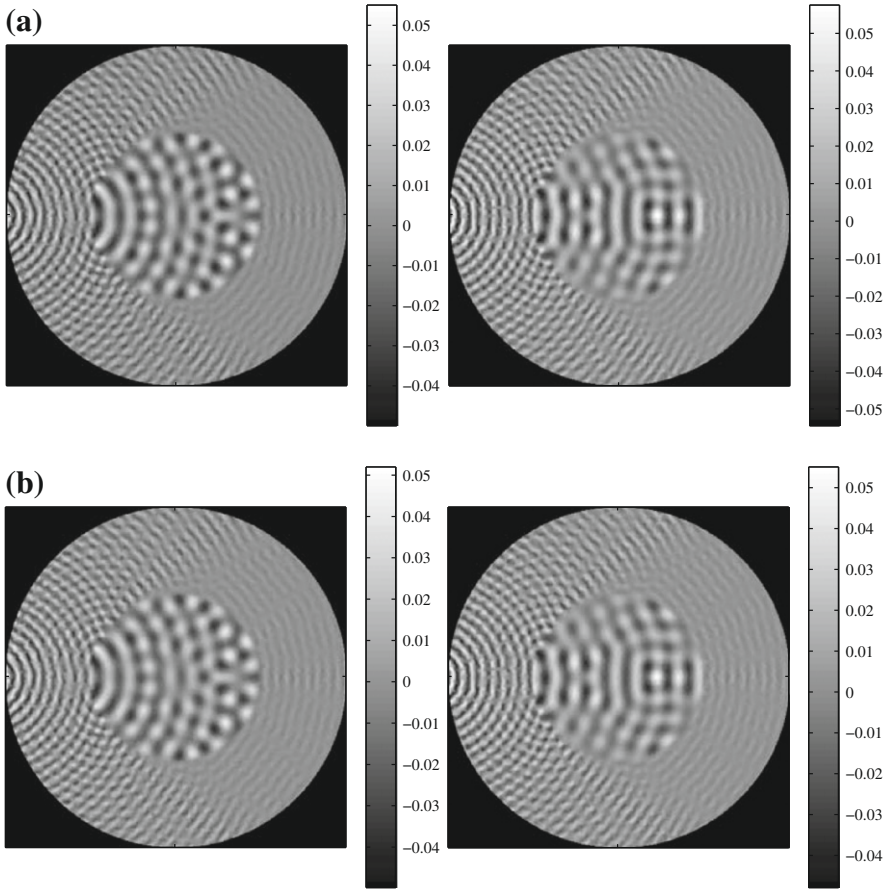

FIGURE 12.5

Cylindrical wave scattered by a circular region of different wave speeds [20]. Top figure (a) shows the analytical solution of the problem with $f = 250$ kHz. Bottom figure (b) shows the UWVF solution of the problem using a uniform basis of 21 wave directions per node. *Reprinted from Ref. [20], with permission from Elsevier.*

governing differential equation exactly. The total potential of the wave, ϕ, is expressed as the sum of the incident potential ϕ^i and the scattered potential, ϕ^s.

$$\phi_k = \phi^i + \phi_k^s = \phi^i + \sum_{j=1}^{m} N_{kj} c_{kj} = \phi^i + \mathbf{N}_k \mathbf{c}_k \tag{12.23}$$

or

$$\phi_k = \sum_{j=1}^{m} N_{kj} c_{kj} = \mathbf{N}_k \mathbf{c}_k \tag{12.24}$$

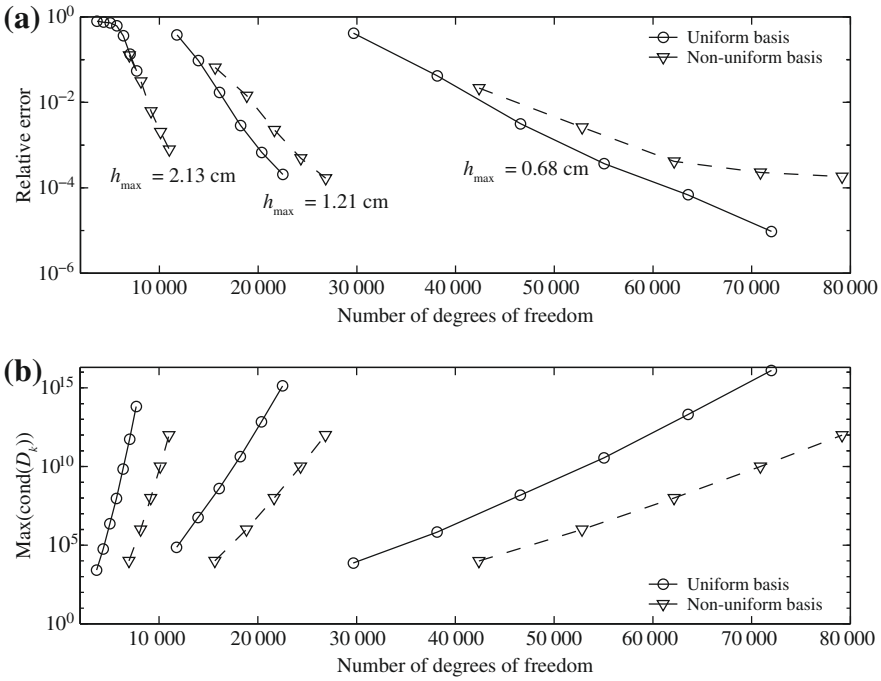

FIGURE 12.6

Relative discrete L_2 errors and condition numbers for three different frequencies against the number of degrees of freedom [20]. Top figure (a) shows the relative discrete L_2 error for three different frequencies against the number of degrees of freedom. Bottom figure (b) shows the condition number. *Reprinted from Ref. [20], with permission from Elsevier.*

where $\mathbf{N}_k$ is a truncated complete set of local solutions to the Helmholtz equation, and $\mathbf{c}_k$ is a set of unknown complex valued coefficients, so that

$$\nabla^2 \mathbf{N}_k + k^2 \mathbf{N}_k = 0 \quad \text{in} \quad \Omega_k \tag{12.25}$$

The corresponding outward normal velocity $v_k = \nabla \phi_k \cdot \mathbf{n}$ on $\partial\Omega_k$ is given by

$$v_k = v^i + \mathbf{T}_k \mathbf{c}_k \quad \text{or} \quad v_k = \mathbf{T}_k \mathbf{c}_k \tag{12.26}$$

The functional to be minimized enforces in a least-squares sense the Neumann boundary conditions on Γ_B and the continuity in potential ϕ and normal derivative v on all the subdomain interfaces, Γ_I. It is given by

$$I(\phi) = I(\mathbf{c}) = w^2 \int_{\Gamma_B} \mid v \mid^2 \, \mathrm{d}\Gamma + \int_{\Gamma_I} \mid \phi_I^+ - \phi_I^- \mid^2 \, \mathrm{d}\Gamma + w^2 \int_{\Gamma_I} \mid v_I^+ + v_I^- \mid^2 \, \mathrm{d}\Gamma \tag{12.27}$$

where the subscripts $+, -$ in integrals along Γ_i indicate solutions from the two respective neighboring Trefftz fields and w is some positive weight. It is assumed that for unbounded domains the selected functions automatically satisfy the Sommerfeld

radiation condition. Setting the first variation of the functional $I(\phi)$ with respect to ϕ equal to zero gives a set of linear equations to solve. Stojek [40] has applied this method to wave scattering problems involving numbers of circular and rectangular cylinders.

12.6.5.1 T-complete systems

The functions used in the various domains of the problem must be complete. They are chosen as follows:

1. Bounded subdomain, Bessel and trigonometric functions:

$$\{J_0(kr),\ J_n(kr)\cos n\theta,\ J_n(kr)\sin n\theta\} \tag{12.28}$$

2. Unbounded subdomain, Hankel and trigonometric functions:

$$\left\{H_0^{(1)}(kr),\ H_n^{(1)}(kr)\cos n\theta,\ H_n^{(1)}(kr)\sin n\theta\right\} \tag{12.29}$$

3. Special-purpose functions for a bounded subdomain with a circular hole, which are linear combinations of the solutions above, satisfying the boundary conditions on the hole of radius b:

$$\left\{\left\{\left(J_0(kr)-\frac{J_0'(kb)}{H_0'(kb)}H_0(kr)\right),\left(J_n(kr)-\frac{J_n'(kb)}{H_n'(kb)}H_n(kr)\right)\cos n\theta,\right.\right.$$
$$\left.\left.\left(J_n(kr)-\frac{J_n'(kb)}{H_n'(kb)}H_n(kr)\right)\sin n\theta\right\}\right\} \tag{12.30}$$

4. Special-purpose functions for the bounded angular corner subdomain:

$$\left\{J_0(kr),\ J_{n/\alpha}(kr)\cos\left[\frac{n}{\alpha}(\theta-\theta_1)\right]\right\} \tag{12.31}$$

where θ_1 is the angle between the straight boundary and the x-axis, and α is the total angle subtended by the angular corner.

12.7 Refraction

As was discussed in Chapter 11, waves can be refracted in two ways:

1. By changes in the local wave speed
2. By movements of the medium through which the waves pass

Examples of the former include transmission of acoustic waves through material with changing density and transmission of surface waves on water of changing depth. Examples of the latter include acoustic waves transmitted through a flow field, like the noise from jet engines and surface waves on ocean, or nearshore currents.

The wave equations take a different form in these two cases. In general the former problem is much simpler than the latter. Conventional finite elements can deal in a straightforward way with refraction caused by changes in the local wave speed,

and no special procedures are needed. The governing equation is simply the inhomogeneous Helmholtz equation and finite elements can solve this just as easily as the homogeneous Helmholtz equation. But for waves refracted by flows, the equation is much more complicated and depends upon the particular application.

12.7.1 Wave speed refraction

The ultra weak variational formulation of Section 12.6.4 above has been applied by Huttunen et al. [20,21] to cases where the wave speed changes between regions of the problem. This is shown in Figs. 12.4–12.6.

Ortiz [43] has extended his method to deal with refracted waves on the surface of water. Ortiz considers an inhomogeneous form of the Helmholtz equation which was developed by Berkhoff [44] for waves on water of gradually changing depth:

$$\nabla \left(A(x, y) \nabla \phi \right) + B(x, y) \phi = 0 \tag{12.32}$$

where

$$\begin{aligned} A(x, y) &= c c_g = \frac{\omega^2}{k^2} \frac{1}{2} \left(1 + \frac{2kh}{\sinh 2kh} \right) \\ B(x, y) &= \omega^2 \frac{c_g}{c} = \omega^2 \frac{1}{2} \left(1 + \frac{2kh}{\sinh 2kh} \right) \end{aligned} \tag{12.33}$$

In this case, strictly speaking, the plane wave basis is no longer valid, since the plane waves are not solutions to the inhomogeneous Helmholtz equation. Ortiz assumes that in each element the plane wave functions still form a valid solution space, since the wave speed does not vary greatly over any element. He modifies the earlier integration scheme [27] to deal with the Berkhoff mild slope wave equation. Again for each pair of wave directions in the element he generates a local coordinate system based on the averaged wave direction. He then integrates analytically in that direction, which contains the most oscillatory variations, and uses conventional integration in the orthogonal direction. His elements are all linear triangles. He uses a Higdon boundary condition to absorb the outgoing waves (see Chapter 11). He presents numerical results for waves scattered by a parabolic shoal and compares them with those of other researchers [43].

The above wave finite elements are strictly only effective for the Helmholtz equation, or other equations with a constant wave speed. The Ortiz formulation is a kind of halfway house, in which the depth is allowed to vary in the governing partial differential equation, but a set of plane waves is still used in the solution space.

Bettess [45] has suggested methods for dealing with refraction. In his proposed method, the wave speed is supposed to vary linearly within triangular elements. It is well known that for a linear variation in the wave speed, waves which are initially plane will follow circular arcs. This effect is used in ray tracing techniques. He therefore proposes to replace the usual set of plane waves with waves following circular arcs. The arc trajectories are relatively straightforward to calculate. Apart from this innovation, the plane wave basis element theory goes over unchanged.

Another possibility which can occur is to have a step change in wave speed. This occurs for example in shallow-water waves where the waves pass over a step, and in elastic waves when there is a discontinuity in the density or stiffness of the elastic material. This is the case modeled by Huttunen et al. [20,21]. The plane wave basis finite elements have recently been extended to deal with this case by Laghrouche et al. [46]. Lagrange multipliers were used to link together the regions with the different wave speeds. The method is as explained by Zienkiewicz et al. [47] Consider a problem in which for simplicity there are only two domains with different wavenumbers, k_1 and k_2. The starting point is the Helmholtz equation

$$(\nabla^2 + k_1^2)\phi_1 = 0 \quad \text{in} \quad \Omega_1 \tag{12.34}$$

We now consider a problem with subdomains with a different constant wave speed in each subdomain. It is sufficient to consider the two-subdomain problem. We begin by considering the solution of the Helmholtz equation expressed in terms of the scalar potential ϕ_1 in the subdomain Ω_1 bounded by $\Gamma_1 \cup \Gamma_{\text{int}}$, where ∇^2 denotes the Laplacian operator and k_1 is the wavenumber in the subdomain Ω_1. Robin boundary conditions are specified on the boundary Γ_1. These are

$$\nabla\phi_1 \cdot \boldsymbol{n}_1 + \mathrm{i}k_1\phi_1 = g_1 \quad \text{on} \quad \Gamma_1 \tag{12.35}$$

where g_1 is the boundary condition, ∇ is the gradient vector operator, and $\boldsymbol{n}_1$ is the outward normal to the line boundary $\Gamma_1 \cup \Gamma_{\text{int}}$.

12.7.1.1 Weighted residual scheme

The differential equation (12.34) is multiplied by an arbitrary weight function W_1 and then integrated by parts to give the weak form

$$B(W_1, \phi_1) = L(W_1) \tag{12.36}$$

where B stands for the bilinear form

$$\begin{aligned} B(W_1, \phi_1) = &\int_{\Omega_1} \left(\nabla W_1 \cdot \nabla\phi_1 - k_1^2 W_1\phi_1\right) \mathrm{d}\Omega \\ &+ \mathrm{i}k_1 \int_{\Gamma_1} W_1\phi_1 \mathrm{d}\Gamma - \int_{\Gamma_{\text{int}}} W_1 \nabla\phi_1 \cdot \boldsymbol{n}_1 \mathrm{d}\Gamma \end{aligned} \tag{12.37}$$

and

$$L(W_1) = \int_{\Gamma_1} W_1 g_1 \mathrm{d}\Gamma \tag{12.38}$$

Following the same procedure, we obtain for the subdomain Ω_2 bounded by $\Gamma_2 \cup \Gamma_{\text{int}}$ the weak form

$$B(W_2, \Phi_2) = L(W_2) \tag{12.39}$$

where all functions and parameters are defined in a similar way as for the weak form (12.36) replacing the subscript 1 by 2.

12.7.1.2 Plane wave basis finite elements

The two subdomains are divided into n-noded finite elements. In each finite element, the potential is first written as a polynomial interpolation of the nodal values of the potential. Then each nodal potential is approximated by a discrete sum of plane waves propagating in different directions in the plane. In our case, a number m_j of plane waves are used in the approximating system at the node j which is similar to that of Eqs. (12.5) and (12.6). Equation (12.5) is retained, but Eq. (12.6) now has different wavenumbers in the two adjacent elements:

$$\psi_1 = e^{\mathrm{i}k_1(x\cos\theta_l + y\sin\theta_l)} \qquad \psi_2 = e^{\mathrm{i}k_2(x\cos\theta_l + y\sin\theta_l)} \tag{12.40}$$

The continuity of potential and the gradient condition are written as follows:

$$\phi_1 = \phi_2 \tag{12.41}$$

and

$$\frac{1}{k_1^2}\nabla\phi_1 \cdot \boldsymbol{n}_1 + \frac{1}{k_2^2}\nabla\phi_2 \cdot \boldsymbol{n}_2 = 0 \tag{12.42}$$

Lagrange multipliers are then introduced to enforce this condition between the two domains, so that

$$\lambda = \frac{1}{k_1^2}\nabla\phi_1 \cdot \boldsymbol{n}_1 = -\frac{1}{k_2^2}\nabla\phi_2 \cdot \boldsymbol{n}_2 \tag{12.43}$$

where $k = \max(k_1, k_2)$ and λ_{jl} are the Lagrange multipliers at node j with respect to direction $\boldsymbol{\xi}_l$. We put $Q_{jl} = N_j \exp(\mathrm{i}k[x\cos\theta_l + y\sin\theta_l])$ and then $\lambda = \boldsymbol{Q}\boldsymbol{\lambda}$. A Galerkin scheme is used so that the weighting functions are chosen to be the same as the interpolating oscillatory functions. The Galerkin equations for the two domains may be written in a matricial form:

$$\begin{aligned} H_1\boldsymbol{A}_1 - C_1\boldsymbol{\lambda} &= \boldsymbol{f}_1 \\ H_2\boldsymbol{A}_2 + C_2\boldsymbol{\lambda} &= \boldsymbol{f}_2 \end{aligned} \tag{12.44}$$

where

$$H_1 = \int_{\Omega_1} \left(\nabla\boldsymbol{P}_1^T\nabla\boldsymbol{P}_1 - k_1^2\boldsymbol{P}_1^T\boldsymbol{P}_1\right)\mathrm{d}\Omega + \mathrm{i}k_1\int_{\Gamma_1}\boldsymbol{P}_1^T\boldsymbol{P}_1\mathrm{d}\Gamma \tag{12.45}$$

$$C_1 = k_1^2\int_{\Gamma_{\mathrm{int}}}\boldsymbol{P}_1^T\boldsymbol{Q}\,\mathrm{d}\Gamma \tag{12.46}$$

and

$$\boldsymbol{f}_1 = \int_{\Gamma_1}\boldsymbol{P}_1^T g_1\mathrm{d}\Gamma \tag{12.47}$$

For the second set of equations in the system (12.44), the matrices are obtained in the same way by replacing subscript 1 by 2. At this stage, there are more unknowns than equations. Therefore, we add the continuity condition as

$$\int_{\Gamma_{\mathrm{int}}}\boldsymbol{Q}^T[\Phi_2 - \Phi_1]\mathrm{d}\Gamma = 0 \tag{12.48}$$

Substituting the approximations for the fields, then writing compactly the above steps gives the following system to solve:

$$\begin{bmatrix} H_1 & 0 & -C_1 \\ 0 & H_2 & C_2 \\ -C_1^T & C_2^T & 0 \end{bmatrix} \begin{Bmatrix} \boldsymbol{A}_1 \\ \boldsymbol{A}_2 \\ \boldsymbol{\lambda} \end{Bmatrix} = \begin{Bmatrix} \boldsymbol{f}_1 \\ \boldsymbol{f}_2 \\ 0 \end{Bmatrix} \tag{12.49}$$

12.7.1.3 *Example problems*

A study of the accuracy of the elements was carried out. When waves pass from a region of slow wave speed to a region of high wave speed, with a large angle between

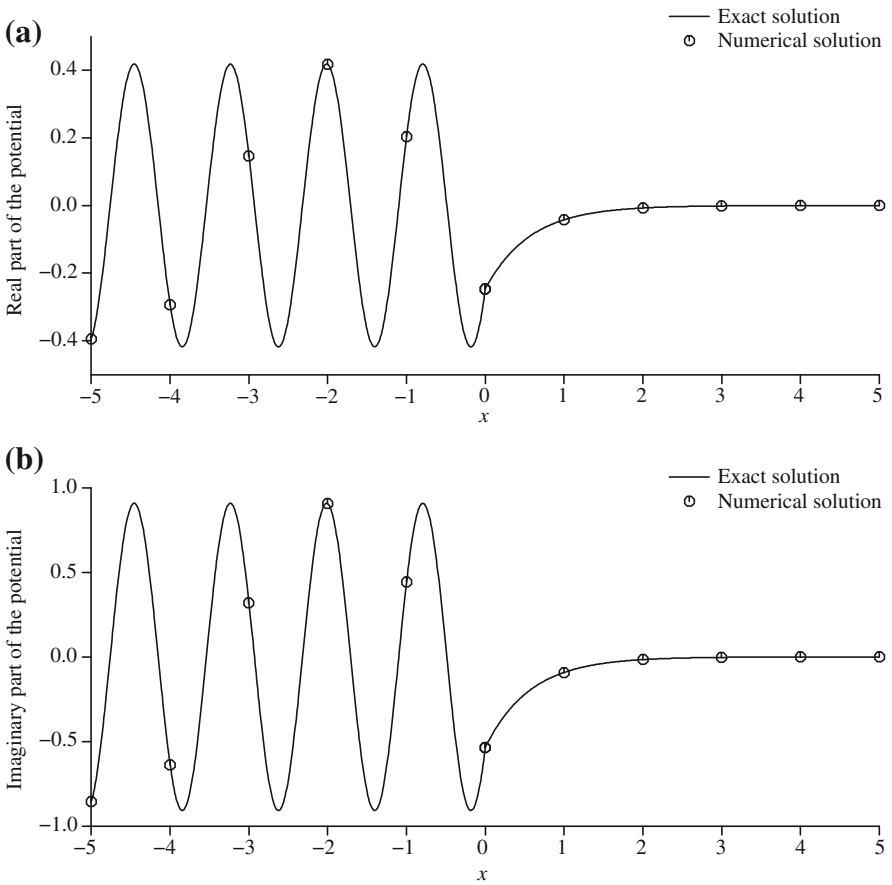

FIGURE 12.7

Evanescent modes, two-subdomain varying wave speed example [46]. Rectangular problem $-5 \leq x \leq 5, -5 \leq x \leq 5$. $k_1, -5 \leq x \leq 0$; $k_2, -5 \leq x \leq 0$. Robin boundary conditions, angle of incidence 45°, critical angle 30°. k_1 and k_2 chosen to give evanescent transmitted wave potential plotted on $y = 0$. *Reproduced by permission of Elsevier.*

the normal to the interface and the direction of wave propagation, edge waves, or evanescent waves, can appear. It is perhaps not obvious that a solution space of plane waves in the plane wave basis elements should be able to accurately represent such evanescent waves, although the proof of completeness would indicate that they should work. Figure 12.7 shows some results where the angle of incidence was chosen to be such that only evanescent waves would arise in the second medium. The element mesh which is not shown is rectangular and appropriate Robin boundary conditions were applied. The plane wave direction set included the incident and reflected wave directions. The results demonstrate that the evanescent effects are properly captured by these elements.

12.7.1.4 Plane scattered by stepped cylinder

This example deals with the diffraction of a plane wave by a rigid circular cylinder, of radius r_1, which is assumed to be vertical, and the plane wave is incident horizontally on the surface of water. Around the cylinder, the water is of depth h_1 up to a circular region of radius r_2. Then for $r \geq r_2$, the depth is h_2. In Fig. 12.8, the outer region is deeper than the one around the cylinder ($h_1 < h_2$). However, the theory remains the same if $h_1 > h_2$. The physical domain of this problem is infinite in extent. This means that it must be truncated at a finite distance from the scatterer to enable a numerical simulation. An analytical solution for the problem in terms of Bessel and Hankel functions was developed in [46]. The problem was analyzed for a range of different k values. The errors are summarized in Table 12.1. ε_2 is the error in the L^2 norm. The parameter τ is the number of degrees of freedom per wavelength.

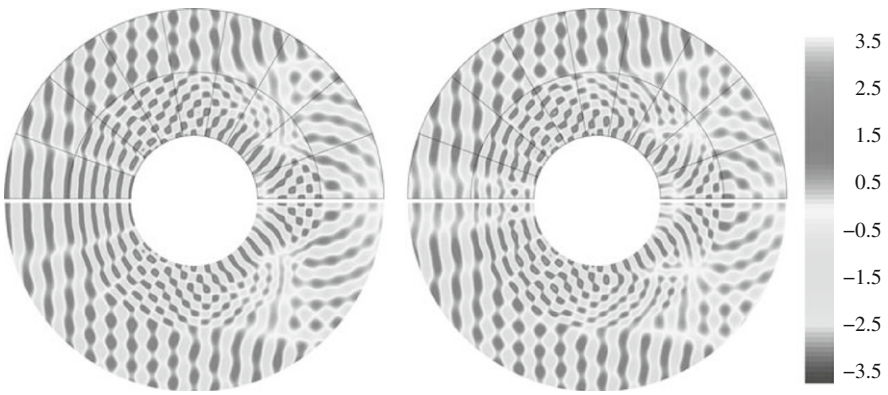

FIGURE 12.8

Waves scattered by stepped cylinder, two-subdomain varying wave speed example [46]. Inner domain: $1 \geq r \geq 2$, $k_1 = 10\pi$, Robin boundary conditions applied and plane wave incident along x-axis. Outer domain: $2 \geq r \geq 3$, $k_2 = 6\pi$. Upper half shows the solution using plane wave basis finite elements and lower half presents plane analytical solution. A total of 3.4 degrees of freedom per wavelength used. L_2 error is 0.4%. *Reproduced by permission of Elsevier.*

Table 12.1 Plane Wave Scattering by a Rigid Circular Cylinder, $k_1 = 2k_2$

k_1	2π	4π	6π	8π	10π	12π	14π	16π	18π	20π
τ	25.9	12.9	8.6	6.5	5.2	4.3	3.7	3.2	2.8	2.6
$\varepsilon_2(\%)$	0.002	0.007	0.02	0.1	0.5	2.5	0.9	0.4	0.6	1.1

Figure 12.8 shows contours of the real and imaginary components of the wave potential around the cylinder for $k_1 = 10\pi$ and $k_2 = 6\pi$. The results are similar to those of Huttunen et al. obtained using the ultra weak variational formulation.

12.7.2 Refraction caused by flows

The problem of waves refracted by flows is more difficult than the case of refraction due to changing wave speed. The topic is dealt with briefly in Chapter 11. Recently Astley and Gamallo [48,49] have applied plane wave basis type methods to wave refraction in the presence of a known flow field in one and two dimensions. In the one-dimensional case the flow is along a duct with changing cross-sectional area. So the flow speed varies with position along the duct. x is the distance along the duct and $A(x)$ is the corresponding cross-sectional area of the duct. The sound speed, $c_0(x)$, the density, $\rho_0(x)$, and the velocity $u_0(x)$ along the duct have been previously found using the one-dimensional nozzle equation. The velocity is given as $u(x) = \mathrm{d}\phi/\mathrm{d}x$, where ϕ is the *acoustic velocity potential*. The governing equation for small acoustic perturbations, derived from the linearized momentum and continuity equations, is then the *convected wave equation*

$$\frac{1}{A\rho_0}\frac{\mathrm{d}}{\mathrm{d}x}\left(\rho_0 A\frac{\mathrm{d}\phi}{\mathrm{d}x}\right)+\frac{\omega^2}{c_0^2}\phi = \mathrm{i}\omega u_0\left(\frac{1}{c_0^2}\frac{\mathrm{d}}{\mathrm{d}x}\left(\frac{\phi}{c_0^2}\right)\right)+u_0\frac{\mathrm{d}}{\mathrm{d}x}\left(\frac{u_0}{c_0^2}\frac{\mathrm{d}\phi}{\mathrm{d}x}\right) \tag{12.50}$$

In the two-dimensional scheme the wavenumber varies in accordance with the prevailing flow. In this case uniform flow in the x-direction, with Mach number M, was considered in a duct, extending from $x = 0$ to $x = L$ and of width a. The resulting convected wave equation in nondimensionalized form is

$$\frac{\partial^2\phi}{\partial^2 y}+(1-M^2)\frac{\partial^2\phi}{\partial^2 x}-2\mathrm{i}kM\frac{\partial\phi}{\partial x}+k^2\phi = 0 \tag{12.51}$$

The specific boundary conditions considered are as follows:

$$(1-M^2)\frac{\partial\phi}{\partial x}-\mathrm{i}kM\phi = -\cos(m\pi y) \quad \text{on} \quad x = 0 \tag{12.52}$$

$$(1-M^2)\frac{\partial\phi}{\partial x}-\mathrm{i}kM\phi = -\mathrm{i}k\phi \quad \text{on} \quad x = L/a \tag{12.53}$$

$$\frac{\partial\phi}{\partial y} = 0 \quad \text{on} \quad y = 0, 1 \tag{12.54}$$

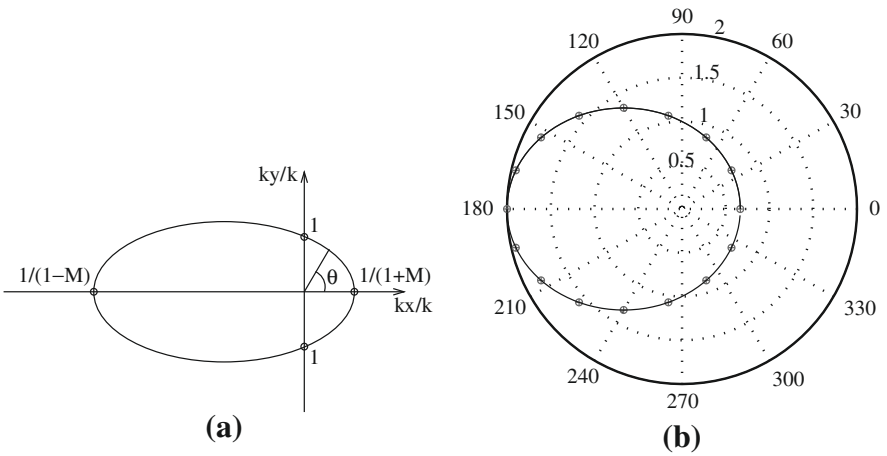

FIGURE 12.9

Wavenumber ellipse for the convective wave equation [49]: (a) the continuous set of wavenumber vectors; (b) a finite set of wavenumber vectors uniformly distributed. *Reproduced by permission from Ref. [49], copyright John Wiley and Sons Ltd.*

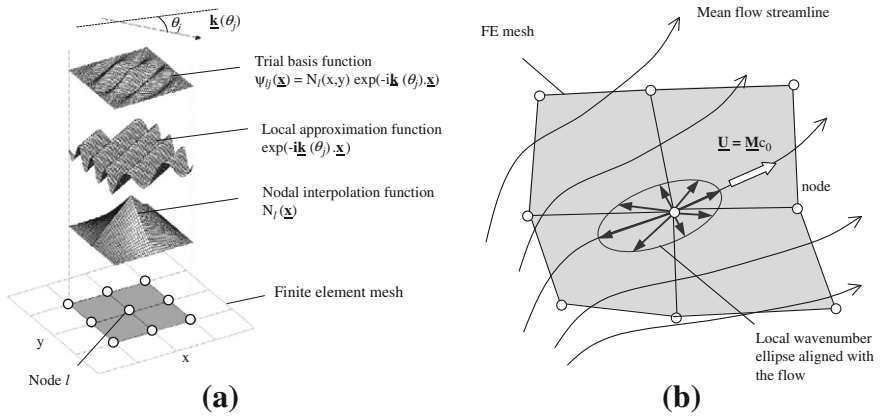

FIGURE 12.10

PUFEM basis [49]: (a) construction of the PUFEM trial basis; (b) the local wavenumber ellipse. *Reproduced by permission from Ref. [49], copyright John Wiley and Sons Ltd.*

A polar plot of the wavenumber as a function of direction at any point takes the form of an ellipse. This is illustrated in Fig. 12.9. The local plane wave basis is also shown in Fig. 12.10. Astley and Gamallo report on the accuracy of the partition of unity elements. In summary they state that "Clearly *all* of the PUM models offer a huge improvement over conventional low order FEM." Astley and Gamallo report the same general experiences as in the zero flow case for such types of element, namely

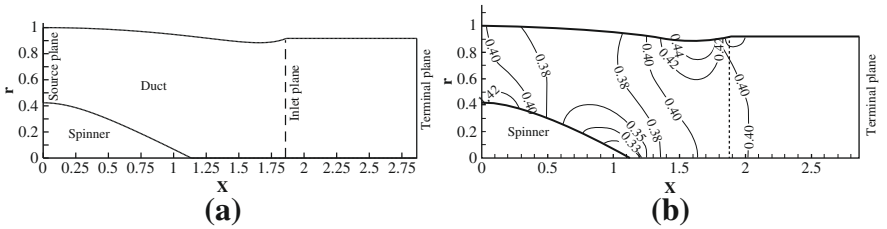

FIGURE 12.11

Nonuniform axisymmetric duct [49]: (a) computational domain; (b) mean flow Mach numbers. *Reproduced by permission from Ref. [49], copyright John Wiley and Sons Ltd.*

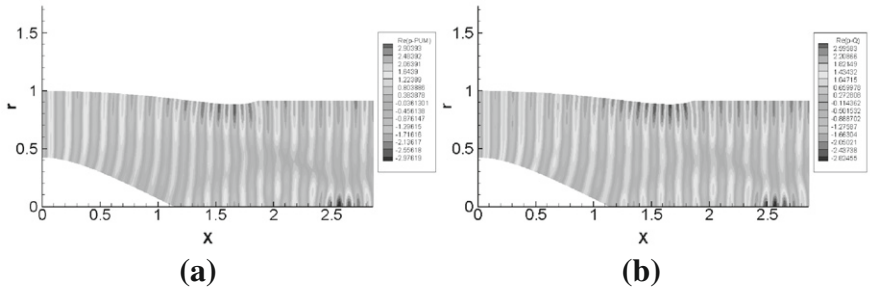

FIGURE 12.12

Nonuniform axisymmetric duct, acoustic pressure field (real part) for $\omega = 25$ [49]: (a) PUFEM, 12,000 degrees of freedom (1500 points and 8 directions); (b) Q-FEM, 100,000 degrees of freedom. *Reproduced by permission from Ref. [49], copyright John Wiley and Sons Ltd.*

reduction in the number of degrees of freedom compared with conventional elements and large condition numbers. The problem of completely general flow fields is more difficult. The plane waves are no longer solutions to the wave pattern in the presence of a general flow field. However they are still a legitimate solution space, though with no guarantee of completeness. The refracted plane wave solutions can still be used on the assumption that they are a good approximation if the flow is not varying rapidly, and is fairly constant locally. Gamallo and Astley [49] have applied the same elements to a general flow field through a nonuniform axisymmetric duct. Figure 12.11 shows the geometry, and Fig. 12.12 shows results obtained using the PUFEM and Q-FEM (quadratic finite elements). They report that accurate solutions are obtained using 12,000 degrees of freedom with PUFEM, whereas 100,000 degrees of freedom are needed for the quadratic conventional finite elements. If the conventional finite element mesh was made any coarser, pollution errors were encountered.

12.8 Spectral finite elements for waves

Spectral finite elements are elements which exploit choices in the selection of the finite element node locations and integration schemes. Conventional consistent mass

matrices lead to a large, though sparse system mass matrix. This is expensive in time-stepping schemes, since even if the time-stepping scheme is explicit the mass matrix has to be factorized and a back substitution carried out at each time step. If the mass matrix is lumped, the formulation is no longer strictly consistent and the results may be unreliable. If it were possible to integrate exactly the mass matrix by sampling only at the nodes within an element, then the mass matrix though theoretically consistent, would be diagonal and explicit time-stepping schemes would be much more economical. If a linear finite element is considered, then the general terms in the mass matrix are quadratic. If a Newton-Cotes formula is used to integrate the mass matrix exactly, then three sampling points are needed in one dimension. As there are only two nodes in a linear element, the number of nodes is inconsistent with an exact integration using a Newton-Cotes integration scheme. If Gauss-Legendre integration is used, then two sampling points are needed to exactly integrate the mass matrix. But these are not at the ends of the element and so the element cannot enforce continuity. However the N point Gauss-Lobatto scheme integrates over the range -1 to $+1$, and samples at the two end points of the range and $N-2$ internal points. The scheme integrates exactly powers of x up to $1+2(N-2)-1=2N-3$, for N sampling points. The scheme comes close to integrating the mass matrix exactly. For example in a one-dimensional quintic finite element with six nodes, the highest power of x in the mass matrix would be 10. The corresponding Gauss-Lobatto scheme would integrate exactly powers of x up to 9. Such integration formulas appear to have been first adopted by Fried and Malkus [50]. They achieved orders of integration, using Gauss-Lobatto schemes which were sufficiently accurate to integrate the stiffness matrix exactly, though not the mass matrix.

The Gauss-Chebyshev scheme also is close to integrating the mass matrix exactly. In both these types of elements the internal nodes of an element are not equally spaced, but are located at the positions dictated by the integration formulas. The Gauss-Legendre-Lobatto scheme is given by

$$\int_{-1}^{+1} f(x)\mathrm{d}x \approx \frac{2}{n(n-1)}\left[f(1)+f(-1)\right]+\sum_{j=2}^{n-1} w_j f(x_j) \tag{12.55}$$

where x_j is the $(j-1)$th zero of $P'_{n-1}(x)$, where $P(x)$ is a Legendre polynomial and the weights, w_j, are given by

$$w_j = \frac{2}{n(n-1)\left[P_{n-1}(x_j)\right]^2} \tag{12.56}$$

The corresponding Gauss-Chebyshev-Lobatto points are given by [50–52]

$$-\cos\frac{\pi i}{N} \tag{12.57}$$

where N is the number of integration points.

The Gauss-Legendre-Lobatto elements have been investigated by Mulder and others [53–55] and the Gauss-Chebyshev-Lobatto elements by Dauksher, Gottlieb,

Hesthaven, and others [51,52,56–62]. There are numerous references to these methods and the above citations are only given as examples of recent work. They are not meant to be exhaustive. In general the numerical investigations demonstrate that spectral elements outperform conventional finite elements in transient wave problems. They have lower dispersion and better phase properties. The Gauss-Chebyshev formulation has also been used for direct collocation approaches to wave problems. This will not be discussed here but references are available [56–62].

In their basic form the spectral elements are not applicable to problems meshed with triangles or tetrahedra. In order to do this, it is necessary to generalize the Gauss-Lobatto and Gauss-Chebyshev-Lobatto schemes to triangles. It is notoriously difficult to generalize integration schemes from straight line segments, squares, and cubes, to triangles and tetrahedra. Although there are proofs that efficient symmetrical integration schemes for triangles and tetrahedral exist there are no general (open-ended) formulas for them, but only special results for certain numbers of points [63,64]. Considerable effort has gone into generalizing the Gauss-Lobatto schemes for triangles and tetrahedra. The corresponding points are called *Fekete* points. The Fekete points are defined as the points which maximize the determinant of the Vandermonde matrix relating the coordinates of the sampling points to the polynomial coefficients. For large numbers of points the interpolating polynomials may become oscillatory and the Vandermonde matrix can become ill-conditioned. The Fekete points are closely related to the Lebesgue points, but are easier to determine [65]. Karniadakis and Sherwin [66] give a very comprehensive treatment of spectral finite elements applied to CFD.

12.9 Discontinuous Galerkin finite elements (DGFE)

This method is frequently used in the time domain, although it can be applied to virtually any finite element problem and not just the Helmholtz wave equation. In the discontinuous Galerkin method, elements are linked together by constraints, which approximately satisfy continuity of various quantities between elements. The jumps between elements are of the same magnitude as the truncation error. The most natural way of applying the constraints is probably the method of Lagrange multipliers. However, this has two disadvantages: the introduction of additional equations to solve, and the indefiniteness of the resulting matrix. In practice the constraints are applied using the element variables themselves. This can be done using some kind of penalty formulation. The mathematical details of the method are explained in Ref. [5]. A comprehensive set of papers on the method edited by Cockburn et al. [67] are available. The paper by Zienkiewicz et al. [47] gives an approachable introduction to the method. The method has been applied to a large range of problems, including waves [68]. Important applications to electromagnetic wave scattering problems are given by Hesthaven and Warburton [69,70]. They explain in considerable detail the techniques needed to extract the full potential of the method. Some of the points are explained below.

A significant property of the discontinuous Galerkin finite element method is that the associated mass matrix is local to each element. Furthermore, the affine nature of straight-sided triangles and tetrahedra implies that their mass matrices differ only by a multiplicative constant. In practical computations, the relatively small reference triangle (or tetrahedron) mass matrix can be inverted in preprocessing, leading to an extremely efficient method. In the conventional finite element method, the assembled stiffness and mass matrices are large sparse matrices, linking together all adjacent degrees of freedom. In the DGFE method the system stiffness matrix need not be formed, and only its product with the vector of field variables from the previous iteration need be retained. This greatly reduces the storage requirement of the method, which becomes $O(N)$, where N is the number of variables in the problem. The other features of the method, as developed by Hesthaven and Warburton and others, are that high-order finite elements are used. They show a 56-node tetrahedron, for example, and use tetrahedra with up to 286 nodes. The node locations are selected using special procedures, and the shape functions are formed using Lagrange polynomial interpolation. Error-bound results, Eq. (12.1), show that for a given number of degrees of freedom in a wave problem, it is better to use higher-order polynomials. The use of higher-order elements involves the use of dense, local, reference element operator matrices. However, in the case of straight-sided triangle meshes only one set of reference operator matrices is required. For a given operation, say differentiation, the reference element matrix is only loaded into cache once and the field data in all elements can be differentiated with this one matrix and then physical derivatives are computed using the chain rule. Coupling this approach with standard, optimized linear algebra mathematics libraries leads to extremely efficient codes.

Exact analytic integration is used where necessary. The authors analyze their scheme for consistency and accuracy. They present a number of results including the scattering of a plane wave by a sphere of radius a at $ka = 10$. Warburton [69] also gives results for the scattering of electromagnetic waves by a F15 fighter aircraft. Results are shown in Figures 12.13 and 12.14.

Eskilsson and Sherwin [68] discuss the modeling of the shallow-water equations using the discontinuous Galerkin method. They consider as an example the modeling of the Port of Visby, on the Baltic Sea. Figure 12.15 shows the mesh of elements which was used and the water depths, and Fig. 12.16 shows a snapshot of the surface elevations after 500 s.

12.10 Concluding remarks

The field of short-wave modeling is currently the focus of intense research activity, not only using finite element, but also boundary integral and other domain and boundary-based methods. At the moment there are a number of promising algorithms, some of which have been described above. The most powerful finite element–based method appears to be the discontinuous Galerkin method. Certainly this has achieved the solution of problems containing the largest number of wavelengths. The other finite element–based algorithms do not seem to be quite so powerful. However given the

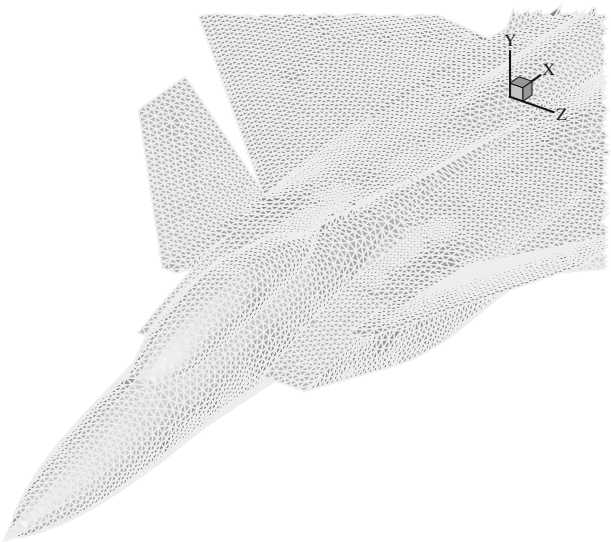

FIGURE 12.13

Electromagnetic waves scattered by fighter aircraft. Projection of finite element mesh onto surface of aircraft. Results due to Hesthaven and Warburton and published in Ref. [61].

Results reproduced with permission from Elsevier.

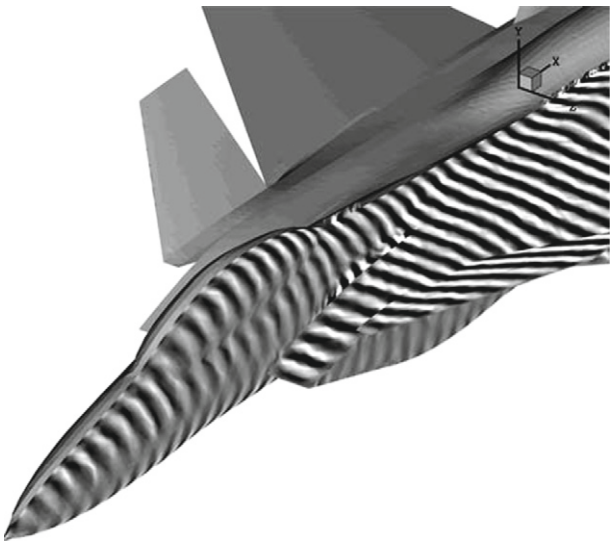

FIGURE 12.14

Electromagnetic waves scattered by fighter aircraft. Contours of electrical field on the surface of aircraft. Results due to Hesthaven and Warburton and published in Ref. [61]

Results reproduced with permission from the publishers.

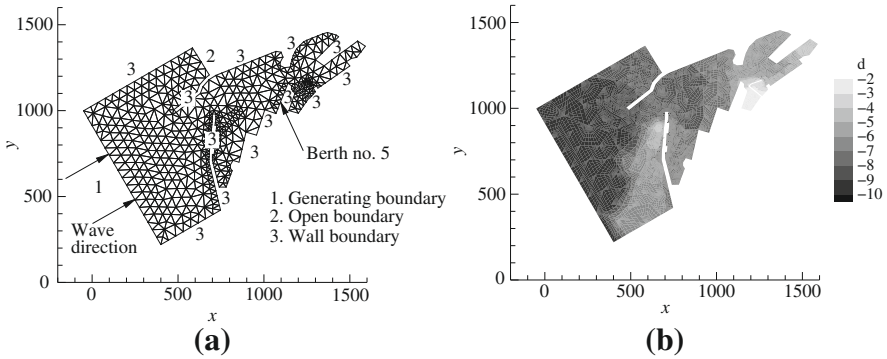

FIGURE 12.15

Harbor layout, Eskilsson and Sherwin [68]: (a) mesh and boundary conditions; (b) depth. *Reproduced by permission from Ref. [68], copyright John Wiley and Sons Ltd.*

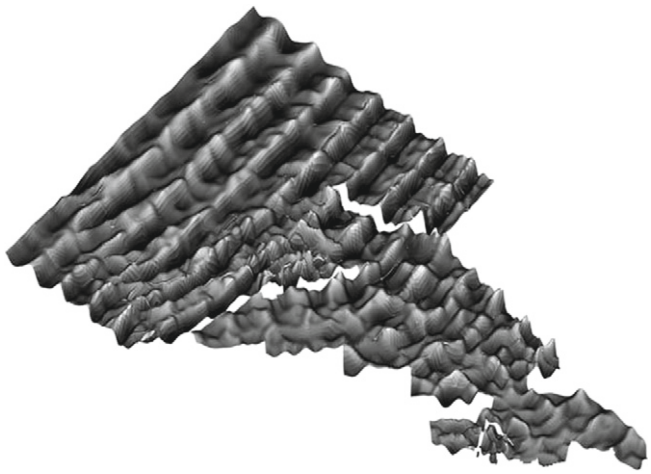

FIGURE 12.16

Snapshot of surface elevation after 500 s [68]. *Reproduced by permission from Ref. [68], copyright John Wiley and Sons Ltd.*

high level of research activity, this may change. The chief competing boundary-based method seems to be the fast multipole method, based on a more efficient formulation of the boundary integral method.

References

[1] P. Bettess, O. Laghrouche, E. Perrey-Debain, Short-wave scattering, Philos. Trans. R. Soc. Ser. A 362 (2004) (Theme Issue).

[2] M. Ainsworth, P. Davies, D. Duncan, P. Martin, B. Rynne, Topics in computational wave propagation, Lecture Notes in Computational Science and Engineering, vol. 51, Springer, Berlin, 2003.
[3] T.J.R. Hughes, Multiscale phenomena: Green's functions, the Dirichlet to Neumann formulation, subgrid scale models, bubbles and the origins of stabilized methods, Comput. Methods Appl. Mech. Eng. 127 (1995) 387–401.
[4] T. Strouboulis, I. Babuška, K. Copps, The design and analysis of the generalised finite element method, Comput. Methods Appl. Mech. Eng. 181 (2000) 43–69.
[5] O.C. Zienkiewicz, R.L. Taylor, J.Z. Zhu, The Finite Element Method: Its Basis and Fundamentals, seventh ed., Elsevier, Oxford, 2013.
[6] F. Ihlenburg, I. Babuška, Dispersion analysis and error estimation of Galerkin finite element methods for the Helmholtz equation, Int. J. Numer. Methods Eng. 38 (1995) 3745–3774.
[7] I. Babuška, F. Ihlenburg, T. Stroubolis, S.K. Gangaraj, A posteriori error estimation for finite element solutions of Helmholtz' equations. Part II: the quality of local indicators and estimators, Int. J. Numer. Methods Eng. 40 (1997) 3443–3462.
[8] I. Babuška, F. Ihlenburg, T. Stroubolis, S.K. Gangaraj, A posteriori error estimation for finite element solutions of Helmholtz' equations. Part II, Int. J. Numer. Methods Eng. 40 (1997) 3883–3900.
[9] M. Ainsworth, Discrete dispersion relation for hp-finite element approximation at high wave number, SIAM J. Numer. Anal. 42 (2004) 553–575.
[10] K. Morgan, O. Hassan, J. Peraire, A time domain unstructured grid approach to the simulation of electromagnetic scattering in piecewise homogeneous media, Comp. Methods Appl. Mech. Eng. 152 (1996) 157–174.
[11] K. Morgan, P.J. Brookes, O. Hassan, N.P. Weatherill, Parallel processing for the simulation of problems involving scattering of electromagnetic waves, Comput. Methods Appl. Mech. Eng. 152 (1998) 157–174.
[12] O.C. Zienkiewicz, P. Bettess, Infinite elements in the study of fluid structure interaction problems, in: Proceedings of the 2nd International Symposium on Computational Methods in Applied Science, Versailles, 1975, in: J. Ehlers et al. (Eds.), Lecture Notes in Physics, vol. 58, Springer-Verlag, Berlin, 1976.
[13] P. Bettess, O.C. Zienkiewicz, Diffraction and refraction of surface waves using finite and infinite elements, Int. J. Num. Methods Eng. 11 (1977) 1271–1290.
[14] R.J. Astley, W. Eversman, A note on the utility of a wave envelope approach in finite element duct transmission studies, J. Sound Vibr. 76 (1981) 595–601.
[15] R.J. Astley, Wave envelope and infinite elements for acoustical radiation, Int. J. Num. Methods Fluids 3 (1983) 507–526.
[16] E. Chadwick, P. Bettess, O. Laghrouche, Diffraction of short waves modelled using new mapped wave envelope finite and infinite elements, Int. J. Numer. Methods Eng. 45 (1999) 335–354.
[17] J.M. Melenk, I. Babuška, The partition of unity finite element method: basic theory and applications, Comput. Methods Appl. Mech. Eng. 139 (1996) 289–314.

[18] J.M. Melenk, I. Babuška, The partition of unity finite element method, Int. J. Numer. Methods Eng. 40 (1997) 727–758.
[19] P.M. Morse, H. Feshbach, Methods of Theoretical Physics, McGraw-Hill, New York, 1953.
[20] T. Huttunen, P. Monk, J.P. Kaipio, Computational aspects of the ultra weak variational formulation, J. Comput. Phys. 182 (2002) 27–46.
[21] T. Huttunen, P. Monk, F. Collino, J.P. Kaipio, Computation aspects of the ultra weak variational formulation, SIAM J. Sci. Comput. 25 (2004) 1717–1742.
[22] P. Mayer, J. Mandel, The finite ray element method for the Helmholtz equation of scattering: first numerical experiments, Technical report, Report Number CU-CAS-00-20, College of Engineering, University of Colorado, Boulder, Colorado, USA. UCD/CCM Report 111, 1997. URL: http://www-math.cudenver.edu/ccm/reports.html.
[23] A. de La Bourdonnaye, High frequency approximation of integral equations modelizing scattering phenomena, Mod. Math. Anal. Numer. 28 (1994) 223–241.
[24] A. de La Bourdonnaye, Convergence of the approximation of wave functions by oscillatory functions in the high frequency limit, C. R. Acad. Paris Sér. I 318 (1994) 765–768.
[25] O. Laghrouche, P. Bettess, Short wave modelling using special finite elements - towards an adaptive approach, in: J.R. Whiteman (Ed.), The Mathematics Finite Elements and Applications X, Elsevier, 2000, pp. 181–194.
[26] O. Laghrouche, P. Bettess, Short wave modelling using special finite elements, J. Comput. Acoust. 8 (2000) 189–210.
[27] P. Ortiz, E. Sanchez, An improved partition of unity finite element model for diffraction problems, Int. J. Numer. Methods Eng. 50 (2001) 2727–2740.
[28] P. Bettess, J. Shirron, O. Laghrouche, B. Peseux, R. Sugimoto, J. Trevelyan, A numerical integration scheme for special finite elements for the Helmholtz equation, Int. J. Numer. Methods Eng. 56 (2002) 531–552.
[29] O. Laghrouche, P. Bettess, E. Perrey-Debain, J. Trevelyan, Plane wave basis for wave scattering in three dimensions, Commun. Numer. Methods Eng. 19 (2003) 715–723.
[30] E. Perrey-Debain, O. Laghrouche, P. Bettess, J. Trevelyan, Plane wave basis finite elements and boundary elements for three dimensions, Philos. Trans. R. Soc. 362 (2004) 561–578, (Theme Issue)
[31] R. Sugimoto, P. Bettess, Coupling of mapped wave infinite elements and plane wave basis finite elements for the Helmholtz equation in exterior domains, Commun. Numer. Methods Eng. 19 (2003) 761–777.
[32] C. Farhat, I. Harari, L. Franca, The discontinuous enrichment method, Report CU-CAS-00-20, Center for Aerospace Structures, University of Colorado, 2000.
[33] C. Farhat, I. Harari, L. Franca, A discontinuous finite element method for the Helmholtz equation, in: Proceedings of the European Congress on Computational Methods in Applied Sciences and Engineering, 2000, ECCOMAS Barcelona, Spain, 11-14 2000, pp. 1–15.

[34] C. Farhat, I. Harari, L. Franca, The discontinuous enrichment method, Comput. Methods Appl. Mech. Eng. 190 (2001) 645–679.
[35] B. Després, Sur une formulation variationelle de type ultra-faible, Comptes Rendus de l'Académie des Sciences-Series I (318) (1994) 939–944.
[36] O. Cessenat, B. Després, Application of an ultra weak variational formulation of elliptic PDEs to the two dimensional Helmholtz problem, SIAM J. Numer. Anal. 35 (1998) 255–299.
[37] J. Jirousek, A. Wróblewski, T-elements: state of the art and future trends, Arch. Comput. Methods Eng. 3 (4) (1996).
[38] I. Herrera, Trefftz method: a general theory, Numer. Methods Partial Differential Equations 16 (2000) 561–580.
[39] J. Jirousek, Basis for development of large finite elements locally satisfying all field equations, Comput. Methods Appl. Mech. Eng. 14 (1978) 65–92.
[40] M. Stojek, Least-squares Trefftz-type elements for the Helmholtz equation, Int. J. Numer. Methods Eng. 41 (1998) 831–849.
[41] I. Herrera, Boundary Methods: An Algebraic Theory, Pitman, London, 1984.
[42] Y.K. Cheung, W.G. Jin, O.C. Zienkiewicz, Solution of Helmholtz equation by the Trefftz method, Int. J. Numer. Methods Eng. 32 (1991) 63–78.
[43] P. Ortiz, Finite elements using plane wave basis, Philos. Trans. R. Soc. 362 (2004) 525–540.
[44] J.C.W. Berkhoff, Refraction and diffraction of waver waves: derivation and method of solution of the two-dimensional refraction-diffraction equation. Report and mathematical investigation, w154, Delft Hydraulics Laboratory, 1973.
[45] P. Bettess, Special wave basis finite elements for very short wave refraction and scattering problems, Commun. Numer. Methods Eng. 20 (2004) 291–298.
[46] O. Laghrouche, P. Bettess, E. Perrey-Debain, J. Trevelyan, Wave interpolation finite elements for Helmholtz problems with jumps in the wave speed, Comput. Methods Appl. Mech. Eng. 194 (2004) 367–381.
[47] O.C. Zienkiewicz, R.L. Taylor, S.J. Sherwin, J. Peiró, On discontinuous Galerkin methods, Int. J. Numer. Methods Eng. 58 (2003) 1119–1148.
[48] R.J. Astley, P. Gamallo, Special short wave elements for flow acoustics, Comput. Methods Appl. Mech. Eng. 194 (2005) 341–353.
[49] P. Gamallo, R.J. Astley, The partition of unity finite element method for short wave acoustic propagation on nonuniform potential flows, Int. J. Numer. Methods Eng. 65 (2006) 425–444.
[50] I. Fried, D.S. Malkus, Finite element mass matrix lumping by numerical integration without convergence rate loss, Int. J. Solids Struct. 11 (1976) 461–466.
[51] W. Dauksher, A.F. Emery, Accuracy in modeling the acoustic wave equation with Chebyshev spectral finite elements, Finite Elem. Anal. Des. 26 (1997) 115–128.
[52] W. Dauksher, A.F. Emery, An evaluation of the cost effectiveness of Chebyshev spectral and p-finite element solutions to the scalar wave equation, Int. J. Numer. Methods Eng. 45 (1999) 1099–1114.

[53] W.A. Mulder, Spurious modes in finite-element discretizations of the wave equation may not be all that bad, Appl. Numer. Math. 30 (1999) 425–445.
[54] W.A. Mulder, Higher-order mass-lumped finite elements for the wave equation, J. Comput. Acoust. 9 (2001) 671–680.
[55] M.J.S. Chin-Joe-Kong, W.A. Mulder, M. Van Veldhuizen, Higher-order triangular and tetrahedral finite elements with mass lumping for solving the wave equation, J. Eng. Math. 35 (1999) 405–426.
[56] J.S. Hesthaven, P.G. Dinesen, J.P. Lynov, Spectral collocation time-domain modeling of diffractive optical elements, J. Comput. Phys. 155 (1999) 287–306.
[57] J.S. Hesthaven, Spectral penalty methods, Appl. Numer. Math. 33 (2000) 23–41.
[58] J.S. Hesthaven, C.H. Teng, Stable spectral methods on tetrahedral elements, SIAM J. Sci. Comput. 21 (2000) 2352–2380.
[59] B. Yang, D. Gottlieb, J.S. Hesthaven, Spectral simulations of electromagnetic waves scattering, J. Comput. Phys. 134 (1997) 216–230.
[60] J.S. Hesthaven, D. Gottlieb, Stable spectral methods for conservation laws on triangles with unstructured grids, Comput. Methods Appl. Mech. Eng. 175 (1999) 361–381.
[61] D. Gottlieb, J.S. Hesthaven, Spectral methods for hyperbolic problems, J. Comput. Appl. Math 128 (2001) 83–131.
[62] J.S. Hesthaven, From electrostatics to almost optimal nodal sets for polynomial interpolation in a simplex, SIAM J. Numer. Anal. 35 (1998) 655–676.
[63] R. Cools, P. Rabinowitz, Monomial cubature rules since 'stroud': a compilation, J. Comput. Appl. Math 48 (1993) 309–326.
[64] R. Cools, Monomial cubature rules since 'Stroud': A compilation–part 2, J. Comput. Appl. Math. 112 (1999) 21–27.
[65] M.A. Taylor, B.A. Wingate, R.E. Vincent, An algorithm for computing Fekete points in the triangle, SIAM J. Numer. Anal 38 (2000) 1707–1720.
[66] G.E. Karniadakis, S.J. Sherwin, Spectral hp Element Methods for CFD, Oxford University Press, Oxford, 1999.
[67] B. Cockburn, G.E. Karniadakis, C.-W. Shu, Discontinuous Galerkin Methods, Springer, Berlin, 2000.
[68] C. Eskilsson, S.J. Sherwin, A triangular spectral/hp discontinuous Galerkin method for modelling 2D shallow water equations, Int. J. Numer. Methods Fluids 45 (2004) 605–624.
[69] T. Warburton, Application of the discontinuous Galerkin method to Maxwell's equations using unstructured polymorphic hp-finite elements, in: B. Cockburn, G.E. Karniadakis, C.-W. Shu (Eds.), Discontinuous Galerkin Methods, Springer, 2000, pp. 451–458.
[70] J.S. Hesthaven, T. Warburton, Nodal high-order methods on unstructured grids-I. Time domain solution of Maxwell's equations, J. Comput. Phys. 181 (2002) 186–221.